PRACTICAL OPTIMIZATION OF REFERENCE-FREE CALIBRATION METHODS FOR DIRECTIONAL DRILLING SENSOR MODULES

Marius V. GHEORGHE[1], Mircea C. BODEA[2]

Despite the abundance of prior work on reference-free calibration methods for inertial and magnetic sensors, very little was written about their optimization. The authors performed an optimization study for the calibration of tilt-compensated compasses in prior work, where they noted that the optimal orientations for the magnetometers and accelerometers are different due the earth magnetic field dip angle. While mathematically optimal, using two sets of orientations increases the total calibration time of directional drilling sensor modules. This paper studies the usage of a common set of orientations, to reduce the calibration time, without degrading the calibration performance.

Keywords: optimization, reference-free calibration

1. Introduction

This paper focuses on advancing the state of the art in the calibration of inertial and magnetic sensors by reducing the total calibration time. Although pragmatic in nature, it addresses the subject using a scientific approach. The work is novel because most prior efforts focus on the development of reference-free algorithms without considering their optimality.

Directional drilling sensor modules consist most frequently of accelerometers and magnetometers, arranged in three orthogonal axes configurations. They are calibrated almost exclusively using reference-free calibration methods, which raises the following main aspects:

- The used algorithm and its ability to perform body frame calibrations.
- The optimality from an error model parameter observability perspective.
- The optimality from a calibration time perspective.

The authors covered in prior work the first two bullet points, advancing the state of the art in each case. However, no prior work references regarding the optimization of the calibration time were found.

[1] Eng. Mgr., Ideal Aerosmith Inc., Phoenix, AZ, USA, e-mail: mgheorghe@idealaero.com
[2] Prof. Em., Faculty of ETTI, University POLITEHNICA of Bucharest, Romania, e-mail: mircea.bodea@upb.ro

The work presented herein focuses on the calibration time optimization without degrading the quality of the calibration. This is an important development with immediate practical application because it results in cost reductions.

This paper is structured as follows:

- Section 1 provides a brief overview of the state of the art, originality, scope, and structure of this paper.
- Section 2 covers the cited references.
- Section 3 introduces notations and conventions used in this paper.
- Section 4 analyzes the first step of a body frame calibration and finds an optimal calibration profile, analytically and through simulation.
- Section 5 analyzes the second and third steps of a body frame calibration and finds an optimal calibration profile, analytically and through simulation.
- Section 6 .. addresses the effectiveness of the proposed method at various dip angles.
- Section 7 .. uses data obtained from the calibration of a commercial directional module to demonstrate that the proposed approach is practical and produces good results.
- .. Section 8 summarizes the salient points of the work presented herein.

2. Prior work

Reference-free calibration methods for inertial and magnetic sensors are frequently covered in papers presented at conferences or published in journals [1] – [18]. However, in most of the cases, little thought is paid to their optimization, turning such methods into sterile theoretical exercises, with limited practical value.

One notable exception is [1], which describes a calibration method widely used in the industry since 1989. Despite its widespread use, this method suffers from the following drawbacks:

- While clever, it is empirical and offers no mathematical guarantees with regards to the best fit of the resulting calibration parameters.
- It does not suggest an implementation method for “kneading” the field such that the lobes are “as equal as possible”, further compounding the shortcoming stated above.
- It does not align the accelerometer and magnetometer tool faces and leaves this important calibration step for future work.
- While it offers intuitions regarding the optimal calibration orientations, it does not demonstrate formally their suitability.
- Finally, it uses a single set of orientations for both accelerometers and magnetometers, without analyzing its optimality.

Reference-free calibration methods that provide body frame calibrations, are presented in [2] and [3], and advance the state of the art versus [1]. The requirement for a minimum number of orientations is clearly identified in these papers, however, no optimization study is performed.

The observability of the error model parameters and its importance in devising a proper calibration scheme are discussed in [4], however, the paper does not provide methods for maximizing or quantifying said observability.

Concerns about the calibration profiles being both sufficient and optimal are stated in [5], however, no solutions to these concerns are provided.

Other papers, such as [6], address the observability of the error model parameters through a brute force approach. While assuring the algorithm convergence, these approaches are anything but optimal from a calibration profile perspective and are not recommended for real-life situations.

In [8] and [9], the calibration profiles are optimal, although that seems to be a happenstance of the used approach: empirical observations in [8] and used apparatus in [9].

Other papers employ random calibration profiles [10] or profiles dictated by the vehicle dynamics [11]. Because of that, they do not guarantee the observability of the calibration parameters, thus cannot guarantee the calibration completion.

In [12] and [13], the authors employ overdetermined but suboptimal calibration profiles. An especially modest performance is shown in [13], perhaps due to the geometric dilution of the calibration parameters observability.

Studies like [14] – [17] offer no explanation about the calibration profiles, and thus no inference could be made about their optimality.

In [18] the authors claim optimality, however, that is a misnomer as the optimality simply refers to the algorithm's ability to converge.

In [19], the authors introduce a rigorous study of the error model parameter observability and provide optimal calibration orientations. The optimization relies on maximizing the partial derivatives of the cost functions used in the calibration. While reducing the calibration time by ensuring that only the minimum number of orientations are used, the approach requires different orientations for the accelerometers and magnetometers, due to the earth magnetic field dip angle.

In the current paper, the authors extend the work introduced in [19], by consolidating the accelerometer and magnetometer calibration profiles to further reduce the calibration duration.

3. Notations and conventions used in this paper

The following notation defines cost functions used in the calibration:

$$f_{\text{sensor,calibration-step}} \tag{1}$$

where: sensor is replaced with G for accelerometers, and H for magnetometers; …calibration − step is replaced with sf for the sensor frame calibration, za for the Z axis alignment, and xa for the X axis alignment (e.g. $f_{\text{G,sf}}$).

The following denotes the sensor frame scale factors and misalignments:

$$m_{\text{sensor,axis1-axis2}} \tag{2}$$

where: sensor is defined as per (1); and axis1 − axis2 could be xx, yy, or zz for the scale factors, and xy, xz, and yz for the misalignments (e.g. $m_{\text{G,xx}}$).

The following denotes the sensor biases:

$$b_{\text{sensor,axis}} \tag{3}$$

where: sensor is defined as per (1); and axis could be x, y, or z (e.g. $b_{\text{G,x}}$).

The following denotes the partial derivative of A with regards to B (e.g. $\partial f_{\text{G,sf}}/\partial m_{\text{G,yz}}$):

$$\partial A/\partial B \tag{4}$$

The following denotes the positioning table's various axes orientations:

$$\alpha_{\text{table-axis}} \tag{5}$$

where: table − axis could be I for the inner axis, M for the middle axis, and O for the outer axis (e.g. α_{I}).

The following denotes the earth magnetic field dip angle:

$$\delta \tag{6}$$

The following denotes the angles by which the sensor triads need to be rotated to align their Z axes to the body reference frame Z axis:

$$\varphi_{\text{sensor}}, \theta_{\text{sensor}} \tag{7}$$

where: φ is the required rotation about the X axis; θ is the required rotation about the Y axis; and sensor is defined as per (1) (e.g. φ_{G}).

The following denotes the angles by which the sensor triads need to be rotated to align their X axes to the body reference frame X axis:

$$\psi_{\text{sensor}} \tag{8}$$

where: ψ is the required rotation about the Z axis; and sensor is defined as per (1) (e.g. ψ_{G}).

The following denotes the absolute normalized value of x over the interval of interest:

$$|x|_{\text{norm}} = |x|/\max(|x|) \tag{9}$$

where: $|x|$ is the absolute value of $|x|$; and $\max(|x|)$ is the maximum absolute value of x over the interval of interest. Applying $|x|_{\text{norm}}$, scales x such that the maximum normalized value becomes 1.

4. Optimization of the sensor frame calibration

This section undertakes to optimize the calibration profiles described in [19], section VI Sensor Frame Calibration. As noted in [2] and [3], this calibration step ortho-normalizes the outputs of the accelerometers and magnetometers and the orientations that represent the best compromise for the accelerometers and magnetometers are those that satisfy the following equations:

$$\left|\partial f_{\text{G,sf}}/\partial m_{\text{G,xx}}\right|_{\text{norm}} = \left|\partial f_{\text{H,sf}}/\partial m_{\text{H,xx}}\right|_{norm} \tag{10}$$

$$\left|\partial f_{\text{G,sf}}/\partial m_{\text{G,xy}}\right|_{\text{norm}} = \left|\partial f_{\text{H,sf}}/\partial m_{\text{H,xy}}\right|_{\text{norm}} \tag{11}$$

$$\left|\partial f_{\text{G,sf}}/\partial m_{\text{G,xz}}\right|_{\text{norm}} = \left|\partial f_{\text{H,sf}}/\partial m_{\text{H,xz}}\right|_{\text{norm}} \tag{12}$$

$$\left|\partial f_{\text{G,sf}}/\partial m_{\text{G,yy}}\right|_{\text{norm}} = \left|\partial f_{\text{H,sf}}/\partial m_{\text{H,zz}}\right|_{\text{norm}} \tag{13}$$

$$\left|\partial f_{\text{G,sf}}/\partial m_{\text{G,yz}}\right|_{\text{norm}} = \left|\partial f_{\text{H,sf}}/\partial m_{\text{H,yz}}\right|_{\text{norm}} \tag{14}$$

$$\left|\partial f_{\text{G,sf}}/\partial m_{\text{G,zz}}\right|_{\text{norm}} = \left|\partial f_{\text{H,sf}}/\partial m_{\text{H,zz}}\right|_{\text{norm}} \tag{15}$$

$$\left|\partial f_{\text{G,sf}}/\partial b_{\text{G,x}}\right|_{\text{norm}} = \left|\partial f_{\text{H,sf}}/\partial b_{\text{H,x}}\right|_{\text{norm}} \tag{16}$$

$$\left|\partial f_{\text{G,sf}}/\partial b_{\text{G,y}}\right|_{\text{norm}} = \left|\partial f_{\text{H,sf}}/\partial b_{\text{H,y}}\right|_{\text{norm}} \tag{17}$$

$$\left|\partial f_{\text{G,sf}}/\partial b_{\text{G,z}}\right|_{\text{norm}} = \left|\partial f_{\text{H,sf}}/\partial b_{\text{H,z}}\right|_{\text{norm}} \tag{18}$$

Substituting (21) – (29) and (38) – (46) from [19] in (10) – (18) above, and solving for α_{M}, where α_{I}, α_{O} are kept at their optimal orientations shown in [19], we obtain the values shown in Table 1

Table 1

Examples of optimal angles for sensor frame calibrations[3]			
Parameter	Accel. optimal $\alpha_{M,G}$	Mag. optimal $\alpha_{M,H}$	Common near-optimal α_M
m_{xx}	90°	$180° - \delta$	98.5°
m_{yy}	90°	$180° - \delta$	98.5°
m_{zz}	45°	$135° - \delta$	53.5°
m_{xy}	90°	$180° - \delta$	98.5°
m_{xz}	45°	$135° - \delta$	53.5°
m_{yz}	180°	$90° - \delta$	98.5°
b_x	90°	$-\delta$	8.5°
b_y	90°	$180° - \delta$	98.5°
b_z	180°	$-(\delta + 90°)$	8.5°

To better evaluate the quality of these findings, the partial derivatives for the accelerometer and magnetometer are graphed side by side in Fig. 1 – Fig. 3.

These graphs show that the crossover points of the red and blue curves are close to their peaks, where their slopes are minimal. Selecting those α_M orientations will not result in a significant geometrical dilution of either partial derivative[4], therefore, the common orientations are near-optimal.

The values illustrated in Table 1 confirm the intuition that a common angle could be obtained by splitting in half the difference between the accelerometer and magnetometer optimal angles and can be computed using the following formula:

$$\alpha_M = (\alpha_{M,G} + \alpha_{M,H})/2 \tag{19}$$

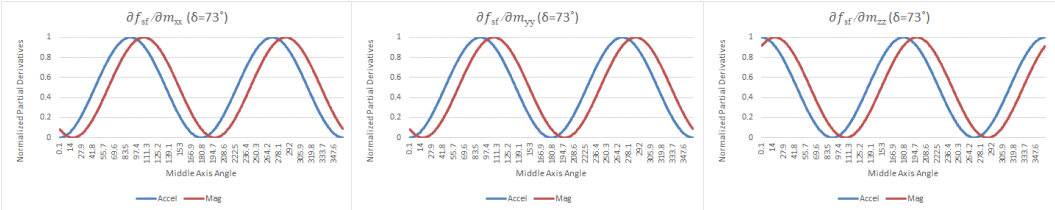

Fig. 1 Partial derivatives corresponding to the scale factors at 73° dip angle

[3] The 73° dip angle value corresponds with the location where the experimental results were obtained: East Grand Forks, Minnesota, USA.

[4] 2.2% for the scale factors, 4.4% for the misalignments, and 1.1% for the biases

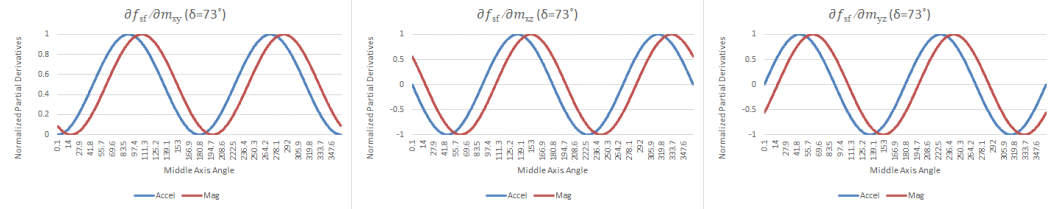

Fig. 2 Partial derivatives corresponding to the misalignments at 73° dip angle

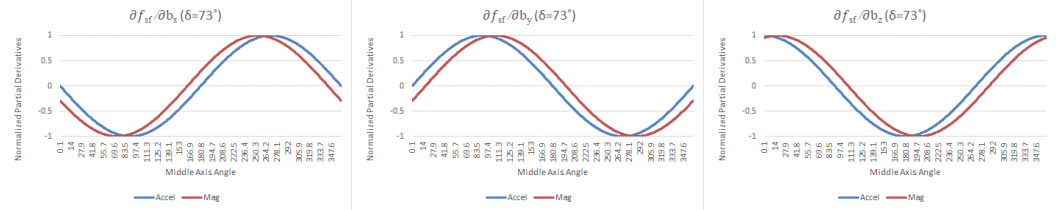

Fig. 3 Partial derivatives corresponding to the biases at 73° dip angle

5. Optimization of the Z & X axes alignment

This section undertakes to optimize the calibration profiles described in [19], sections VII Z Axis Alignment and VIII X Axis Alignment. As noted in [2] and [3], these calibration steps align the Z axes of the ortho-normalized accelerometer and magnetometer sensor frames to the body frame Z axis, and the X axes of the accelerometer and magnetometer, respectively.

The orientations that represent the best compromise for the accelerometers and magnetometer are those that satisfy the following equations:

$$\partial f_{\mathrm{G,za}}/\partial \varphi_{\mathrm{G}} = \partial f_{\mathrm{H,za}}/\partial \varphi_{\mathrm{H}} \tag{20}$$

$$\partial f_{\mathrm{G,za}}/\partial \theta_{\mathrm{G}} = \partial f_{\mathrm{H,za}}/\partial \theta_{\mathrm{H}} \tag{21}$$

$$\partial f_{\mathrm{G,xa}}/\partial \psi_{\mathrm{G}} = \partial f_{\mathrm{H,xa}}/\partial \psi_{\mathrm{H}} \tag{22}$$

Substituting (48), (49), (51), (52), (54), and (56) from [19] in (20) – (22) above, and solving for α_{M}, where α_{I} and α_{O} are kept at their optimal orientations shown in [19], we obtain the values shown in Table 2 and Table 3.

To better evaluate the quality of these findings, the partial derivatives for the accelerometer and magnetometer are graphed side by side in Fig. 4 and Fig. 5. These graphs show that, for the given dip angle, the crossover points of the red and blue curves are close to their peaks, where their slopes are minimal. Selecting

those α_M orientations will not result in a significant geometrical dilution[5], therefore, the common orientations are near-optimal.

Table 2

Examples of optimal angles for Z axis alignment[6]			
Parameter	Accel. optimal $\alpha_{M,G}$	Mag. optimal $\alpha_{M,H}$	Common near-optimal α_M
φ	90°	$180° - \delta$	98.5°
θ	90°	$180° - \delta$	98.5°

Table 3

Examples of optimal angles for X axis alignment[7]			
Parameter	Accel. optimal $\alpha_{M,G}$	Mag. optimal $\alpha_{M,H}$	Common near-optimal α_M
ψ	90°	$180° - \delta$	98.5°

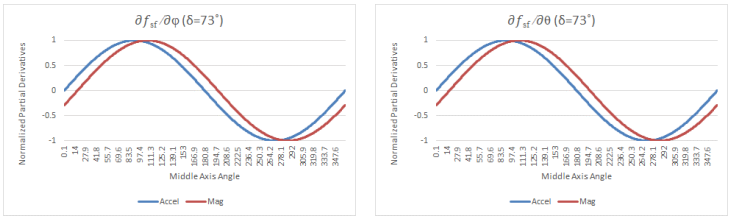

Fig. 4 Partial derivatives corresponding to the φ and θ rotations at 73° dip angle

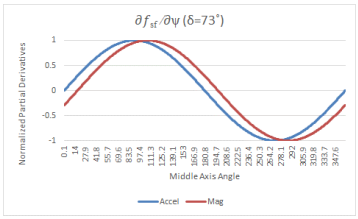

Fig. 5 Partial derivative corresponding to the ψ rotation at 73° dip angle

The values of the common angles obtained shown in Table 2 and Table 3 confirm the intuition of splitting the difference in half, and conform to (19).

[5] The dilution of the partial derivatives is just 1.1% for either angle.

[6] The 73˚ dip angle value corresponds with the location where the experimental results were obtained: East Grand Forks, Minnesota, USA.

[7] The 73˚ dip angle value corresponds with the location where the experimental results were obtained: East Grand Forks, Minnesota, USA.

6. Other dip angles of interest

So far, the dip angle corresponded to the location where the experimental data was collected. For other locations, only simulation results will be presented.

For locations close to the poles, ($\delta = \pm 90°$) and the equator ($\delta = \pm 0°$), the orientations optimal for the magnetometer coincide with those optimal for the accelerometer ones due to spatial periodicity.

Therefore, it stands to reason that the worst-case scenario is half-way in between ($\delta = \pm 45^{\circ}$). Sample graphs for this dip angle are shown in Fig. 6 – Fig. 7.

The sample crossovers shown in Fig. 6 and Fig. 7 are worse than the ones shown before[8,9]. The impact of performing the calibration at this dip angle on the algorithms' ability to converge, and on the accuracy of the calibration parameters will be left for a future analysis[10].

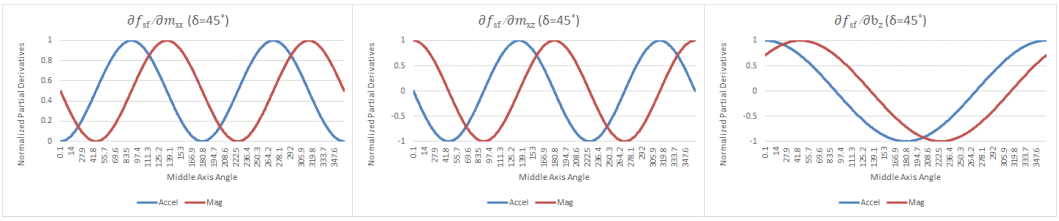

Fig. 6 Partial derivatives corresponding to sensor frame calibration coefficients at 45° dip angle

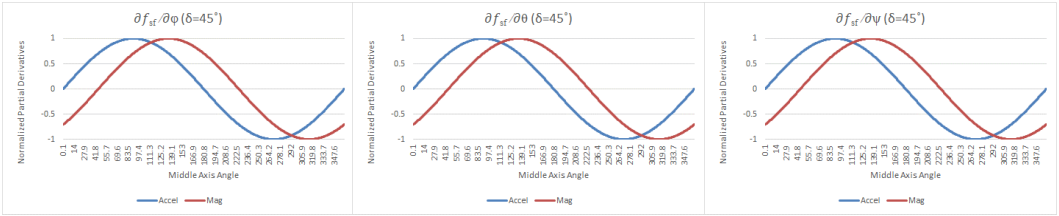

Fig. 7 Partial derivatives corresponding to the φ, θ, and ψ rotations at 45° dip angle

[8] 14.6% dilution for the scale factors, 29.3% for the misalignments, and 7.6% for the biases.

[9] 7.6% dilution for the rotation angles.

[10] By comparison, a dip angle of 61°50′, corresponding to Bucharest, Romania, will cause a 5.9% geometrical dilution of the partial derivatives corresponding to the scale factors, a maximum 11.8% for the misalignments, and 3.0% for the biases and axis alignment angles.

7. Experimental data

Data was collected from a General Electric directional sensor module using a non-magnetic positioning table, model 2203-TH-NM, in East Grand Forks, Minnesota, USA, in a non-magnetic calibration laboratory.

Two sets of data were collected:

- Data corresponding to a dual set of optimal orientations, one for the accelerometers and one for the magnetometers.
- Data corresponding to single set of near-optimal orientations, common to both accelerometers and magnetometers.

Full body frame calibrations, involving sensor frame calibrations, Z and X axes alignments were performed on both data sets and the results compared.

One method of evaluating the effectiveness of the near-optimal calibration orientations is to compare the moduli of the gravitational and magnetic fields, computed from the corrected sensor readings, against the known values of those fields (see Fig. 8). These graphs show that the performance of the sensor module in estimating the total fields is very similar, regardless of the calibration scenario.

Fig. 8 Gravitational and magnetic fields moduli errors

A second way of estimating the performance is to compare the results of a roll test performed by rotating the sensor module around its Z axis while keeping its attitude and heading unchanged. The accelerometer readings are then used to compute the sensor module's inclination using the following formula:

$$I_G = \cos^{-1}\left(\frac{X_{G,corr}}{\sqrt{X_{G,corr}^2 + Y_{G,corr}^2 + Z_{G,corr}^2}}\right) \tag{23}$$

where: I_G is the sensor module's inclination; and $X_{G,corr}$, $Y_{G,corr}$, and $Z_{G,corr}$ are the accelerometer corrected readings for the three axes.

Although not directly useful for directional drilling, (23) can also be applied by extension to the magnetometer, solely for evaluating the calibration performance. The results of the roll test are shown in Fig. 9 and demonstrate that the performance is similar for the two calibration scenarios.

A third way of assessing the calibration performance is to compute the dip angle from the corrected sensor readings using the following formula:

$$\delta = \sin^{-1}\left(\frac{X_{G,corr}X_{H,corr} + Y_{G,corr}Y_{H,corr} + Z_{G,corr}Z_{H,corr}}{\sqrt{X_{G,corr}^2 + Y_{G,corr}^2 + Z_{G,corr}^2}\sqrt{X_{H,corr}^2 + Y_{H,corr}^2 + Z_{H,corr}^2}}\right) \quad (24)$$

The dip angle graphs are shown in Fig. 10 and demonstrate that the performance is similar for the two calibration scenarios.

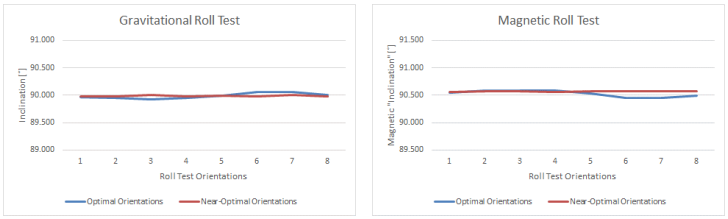

Fig. 9 Roll test results

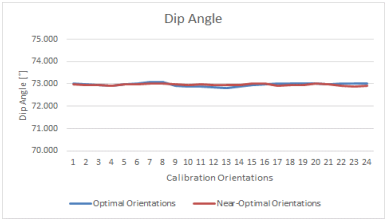

Fig. 10 Dip angle

8. Conclusions

This paper addresses a subject not covered elsewhere in literature and finds both analytically and through simulation near-optimal orientations that can be used to reduce the calibration time for sensor modules used in directional drilling, an important consideration in real-life applications. The theoretical and simulation results were verified through experimentation and the optimization approach is expected to be incorporated in a commercial project.

R E F E R E N C E S

[1] *R. Estes, P. Walters,* "Improvement of Azimuth Accuracy by Use of Iterative Total Field Calibration Technique and Compensation for System Environment Effects", Society of Petroleum Engineers Annual Technical Conference, Oct. 1989, pp. 287-298.

[2] *M. V. Gheorghe,* "Calibration for Tilt-Compensated Electronic Compasses with Alignment between the Magnetometer and Accelerometer Sensor Reference Frames", International

Instrumentation & Measurement Technology Conference (I2MTC2017), proceedings, pp. 862-867.
[3] *M. V. Gheorghe,* "Advanced Calibration Method for 3-Axis MEMS Accelerometers", International Semiconductor Conference, CAS 2016, pp. 81-84.
[4] *P. Gao, K. Li, L. Wang, Z. Liu,* "A Self-Calibration Method for Accelerometer Nonlinearity Errors in Triaxis Rotational Inertial Navigation System", IEEE Transactions on Instrumentation and Measurement, Feb. 2017, vol. **66**, iss. 2, pp. 243-253.
[5] *P. Schopp, H. Graf, W. Burgard, Y. Manoli*, "Self-Calibration of Accelerometer Arrays", IEEE Transactions on Instrumentation and Measurement, Aug. 2016, vol. **65**, iss. 8, pp. 1913-1925.
[6] *C. Wang, X. Qu, X. Zhang, W. Zhu, G. Fang,* "A Fast Calibration Method for Magnetometer Array and the Application of Ferromagnetic Target Localization", IEEE Transactions on Instrumentation and Measurement, Jul. 2017, vol. **66**, iss. 7, pp. 1743-1750.
[7] *J. Fang, Z. Liu*, "A New Inclination Error Calibration Method of Motion Table Based on Accelerometers", IEEE Transactions on Instrumentation and Measurement, Feb. 2015, vol. **64**, iss. 2, pp. 487-493.
[8] *L. Ye, Y. Guo, S. W. Su*, "An Efficient Autocalibration Method for Triaxial Accelerometer", IEEE Transactions on Instrumentation and Measurement, 2017, vol. **PP**, iss. 99, pp. 1-11.
[9] *O. Särkkä, T. Nieminen, S. Suuriniemi, L. Kettuen,* "A Multi-Position Calibration Method for Consumer-Grade Accelerometers, Gyroscopes, and Magnetometers to Field Conditions", IEEE Sensors Journal, Jun. 2017, vol. **17**, no. 11, pp. 3470-3481.
[10] *Z. Q. Zhang,* "Cameras and Inertial-Magnetic Sensor Units Alignment Calibration", IEEE Transactions on Instrumentation and Measurement, Jun. 2016, vol. **65**, iss. 6, pp. 1495-1502.
[11] *Y. Stebler, S. Guerrier, J. Skaloud,* "An Approach for Observing and Modeling Errors in MEMS-Based Inertial Sensors Under Vehicle Dynamic", IEEE Transactions on Instrumentation and Measurement, Nov. 2015, vol. **64**, iss. 11, pp. 2926-2936.
[12] *J. Rohac, M. Sipos, J. Simanek,* "Calibration of Low-cost Triaxial Inertial Sensors", IEEE Instrumentation & Measurement Magazine, Dec. 2015, vol. **18**, iss. 6, pp. 32-38.
[13] *B. Li, J. Lu, W. Xiao, T. Lin,* "In-field fast calibration of FOG-based MWD IMU for horizontal drilling", Measurement Science and Technology Journal, Jan. 2015, no. 27, pp. 1-7.
[14] *S. Guerrier, R. Molinari, Y. Stebler,* "Wavelet-Based Improvements for Inertial Sensor Error Modeling", IEEE Transactions on Instrumentation and Measurement, Dec. 2016, vol. **65**, iss. 12, pp. 2693-2700.
[15] *G. Panahandeh, M. Jansson, P. Händel,* "Calibration of an IMU-Camera Cluster Using Planar Mirror Reflection and Its Observability Analysis", IEEE Transactions on Instrumentation and Measurement, Jan. 2015, vol. **64**, iss. 1, pp. 75-88.
[16] *A. Zikmund, M. Janosek, M. Ulvr, J. Kupec,* "Precise Calibration Method for Triaxial Magnetometers Not Requiring Earth's Field Compensation", IEEE Transactions on Instrumentation and Measurement, May 2015, vol. **64**, iss. 5, pp. 1242-1247.
[17] *P. Daponte, L. De Vito, G. Mazzilli, F. Picariello, S. Rapuano*, "Method for compensating the effect of disturbances on magnetometer measurements: experimental results", Instrumentation and Measurement Technology Conference (I2MTC), May 2017, Proceedings of, pp. 1864-1869.
[18] *Y. Gao, L. Guan, T. Wang,* "Optimal artificial fish swarm algorithm for the field calibration on marine navigation", Measurement, vol. **50**, Apr. 2014, pp. 297-304.
[19] *M. V Gheorghe, M. C. Bodea*, "Calibration Optimization Study for Tilt-Compensated Compasses", in print, IEEE Transactions on Instrumentation and Measurement.
[20] *S. Gratton, A.S. Lawless, N.K. Nichols,* "Approximate Gauss-Newton methods for nonlinear least squares problems", SIAM Journal on Optimization (SIOPT), vol. **18**, no. 1, pp. 106-132.